

^{139}La NMR investigation of the interplay between the lattice, charge, and spin dynamics in charge ordered high T_c cuprate $\text{La}_{1.875}\text{Ba}_{0.125}\text{CuO}_4$

P. M. Singer¹, A. Arsenault², T. Imai², and M. Fujita³

¹*Department of Chemical and Biomolecular Engineering,*

Rice University, 6100 Main St., Houston, TX 77005-1892, United States

²*Department of Physics and Astronomy, McMaster University, Hamilton, Ontario, L8S 4M1, Canada and*

³*Institute for Materials Research, Tohoku University, Sendai 980-8577, Japan*

(Dated: March 21, 2024)

We investigate the interplay between the lattice, charge, and spin dynamics in charge ordered high T_c cuprate $\text{La}_{1.875}\text{Ba}_{0.125}\text{CuO}_4$ ($T_c = 4$ K) based on the inverse Laplace transform (ILT) analysis of the ^{139}La nuclear spin-lattice relaxation rate $1/T_1$ (dubbed ILTT₁ analysis here after). A major thrust of the ILTT₁ analysis is that one can deduce the probability density function $P(1/T_1)$ of distributed $1/T_1$. We demonstrate that $1/T_1^{lm}$, defined as the log-mean (i.e. the center of gravity on a logarithmic scale) of $P(1/T_1)$, can be well approximated by $1/T_1^{str}$ deduced from the phenomenological stretched fit, however, $P(1/T_1)$ can provide much richer insight into how the lattice, charge, and spin fluctuations and their distribution develop near and below the long range charge order at $T_{charge} \sim 54$ K. Upon entering the charge ordered state, a divergent increase of $1/T_1^{lm}$ toward the spin ordering at $T_{spin}^{\mu SR} \simeq 35$ K is accompanied by an asymmetric broadening of $P(1/T_1)$. Even deep inside the charge ordered state, $1/T_1$ at a gradually diminishing fraction of ^{139}La sites continues to slow down as temperature is lowered, as expected for canonical superconducting CuO_2 planes without enhanced spin fluctuations. The fraction of such canonical ^{139}La sites almost disappears by $\simeq 40$ K. In contrast, nearly a half of the ^{139}La sites in $\text{La}_{1.885}\text{Sr}_{0.115}\text{CuO}_4$ ($T_{charge} \simeq 80$ K) still exhibits the canonical behavior without enhanced spin fluctuations even near its $T_c = 31$ K. These contrasting behaviors explain why superconductivity in $\text{La}_{1.875}\text{Ba}_{0.125}\text{CuO}_4$ is more strongly suppressed than in $\text{La}_{1.885}\text{Sr}_{0.115}\text{CuO}_4$ despite the lower onset temperature of the charge order.

I. GENERAL INTRODUCTION

In $\text{La}_{2-x}\text{Sr}_x\text{CuO}_4$, the high temperature superconducting phase with the critical temperature as high as $T_c = 38$ K manifests itself after the high temperature tetragonal (HTT) to low temperature orthorhombic (LTO) structural phase transition takes place around $\simeq 200$ K. In contrast, $\text{La}_{2-x}\text{Ba}_x\text{CuO}_4$ undergoes an additional structural phase transition from the LTO to the low temperature tetragonal (LTT) phase below $T_{LTO-LTT} \simeq 60$ K, and T_c in the LTT structure is anomalously suppressed to as low as $T_c \simeq 4$ K near the magic composition with $x \simeq 1/8$ [1]. μSR measurements uncovered the presence of spin order below $T_{spin}^{\mu SR} \simeq 35$ K in $\text{La}_{1.875}\text{Ba}_{0.125}\text{CuO}_4$ [2].

Nd co-doping into $\text{La}_{2-x}\text{Sr}_x\text{CuO}_4$ also induces the same sequence of structural transitions from HTT to LTO, and then to LTT. It was in $\text{La}_{1.48}\text{Nd}_{0.4}\text{Sr}_{0.12}\text{CuO}_4$ where Tranquada et al. [3] discovered the charge order transition at $T_{charge} \simeq 60$ K in the LTT phase based on neutron diffraction measurements. Subsequent NMR [4, 5] and neutron scattering experiments [6] showed that a charge order transition accompanies the LTO to LTT structural transition also in $\text{La}_{1.875}\text{Ba}_{0.125}\text{CuO}_4$. More recently, x-ray scattering experiments [7, 8] revealed the presence of dynamic short range charge order in $\text{La}_{1.875}\text{Ba}_{0.125}\text{CuO}_4$ prior to the onset of long range charge order at $T_{charge} \simeq 54$ K [8].

There has been a long history in the NMR investigation of the complicated behavior of $\text{La}_{2-x}\text{Ba}_x\text{CuO}_4$

[4, 5, 9–15], yet our understanding of the interplay between the lattice, charge, and spin degrees of freedom near charge order is still far from complete. This is in part because the NMR spin-lattice relaxation rate $1/T_1$ develops a large distribution near and below T_{charge} , and the NMR community in condensed matter physics did not have the machinery to accurately probe the nature and extent of the distribution. Furthermore, the phenomenological approach to deduce $1/T_1$ based on the stretched exponential fit of the nuclear spin recovery curve $M(t)$ cannot distinguish the fluctuations of the electric field gradient (EFG) and spins.

In this paper, we shed new light on the complex behavior of $\text{La}_{1.875}\text{Ba}_{0.125}\text{CuO}_4$ by analyzing the $1/T_1$ recovery curve $M(t)$ observed at the ^{139}La sites based on the inverse Laplace transform (ILT) analysis techniques (dubbed *ILTT₁ analysis* hereafter). The ILT in the context of NMR has been conceptually known for some time [16], and applied successfully in petrophysics [17–21] and condensed matter physics [22, 23] by numerically inverting $M(t)$. A major thrust of the ILTT₁ analysis is that *one can generate the histogram of distributed $1/T_1$ without presuming any particular functional form of the density function $P(1/T_1)$* , in addition to the log-mean $1/T_1^{lm}$ (i.e. the center of gravity on a logarithmic scale) of the distributed relaxation rate. We will demonstrate that slow lattice and/or charge fluctuations develop at the NMR frequency scales below $\simeq 80$ K, where the dynamic short range charge order develops [8]. Comparison of $P(1/T_1)$ between $\text{La}_{1.875}\text{Ba}_{0.125}\text{CuO}_4$ ($T_c = 4$ K) and $\text{La}_{1.885}\text{Sr}_{0.115}\text{CuO}_4$ ($T_c \simeq 31$ K) also reveals a qualita-

tive difference between the two. The volume fraction of the canonically superconducting domains in the CuO_2 planes without enhanced spin fluctuations is reduced to almost null in $\text{La}_{1.875}\text{Ba}_{0.125}\text{CuO}_4$ below $\simeq 40$ K, whereas nearly a half of the volume still behaves as a canonical superconductor in $\text{La}_{1.885}\text{Sr}_{0.115}\text{CuO}_4$.

The rest of this paper is organized as follows. In section II, we explain the key aspects of the ILT techniques and what the ILTT₁ analysis can (not) do. Section III outlines the experimental methods, and section IV discusses the results, followed by summary and conclusions in section V.

II. INVERSE LAPLACE TRANSFORM OF $M(t)$

To measure the spin-lattice relaxation time T_1 , one applies an inversion pulse and monitors the recovery curve $M(t)$ of the nuclear magnetization as a function of time t . In the simplest case of nuclear spin $I = 1/2$ with a single, non-distributed value of $1/T_1$, the recovery obeys an exponential form as such:

$$M(t) = M_0 - A e^{-t/T_1}, \quad (1)$$

where M_0 is the saturated value of the nuclear magnetization, and A ($\leq 2M_0$) represents the degree of inversion.

Magnetic inhomogeneity of the sample results in a distribution of $1/T_1$, and $M(t)$ may exhibit a stretched exponential form under certain circumstances [16, 24, 25],

$$M(t) = M_0 - A e^{-(t/T_1^{str})^\beta}, \quad (2)$$

where β is the stretched exponent less than 1. If $1/T_1$ has no distribution, $1/T_1^{str} = 1/T_1$ and $\beta = 1$. For example, in the case of $1/T_1$ measured by ^{63}Cu nuclear quadrupole resonance (NQR) techniques in a highly disordered $\text{YBa}_2\text{Cu}_3\text{O}_{6.9}$ sample ($T_c = 92$ K), Eq. (2) worked well far below T_c with the exponent $\beta = 1/2$ [26], which is expected for diffusion-less, enhanced relaxation caused by defect spins [24, 25]. One can justify such a stretched fit, if $\ln[M_0 - M(t)]$ vs. t^β or $\ln[M_0 - M(t)]$ vs. $\ln(t)$ yields a straight line [24, 26].

One needs to bear in mind that the distributed relaxation mechanisms do not always lead to the stretched form in Eq. (2). In fact, Eq. (2) failed for $\text{YBa}_2\text{Cu}_3\text{O}_{6.95}$ ($T_c = 92$ K) with less magnetic defects [27, 28]. Instead, a two component fit worked well, with two distinct values of fast and slow relaxation rates, $1/T_1^{fast}$ and $1/T_1^{slow}$:

$$M(t) = M_0 - A_{fast} e^{-t/T_1^{fast}} - A_{slow} e^{-t/T_1^{slow}}. \quad (3)$$

In this case, dilute defect spins affect only the nuclear spins in their vicinity, and the rest of the superconductor exhibit much longer, intrinsic $1/T_1^{slow}$. An analogous situation arises for $1/T_1$ measured for type II superconductors under the presence of vortex cores induced by an external magnetic field. Accordingly, in NMR research on

superconductivity, it is usually $1/T_1^{slow}$ that researchers present far below T_c .

A dilemma arises if there is no clearcut justification for Eq. (2) or (3). In fact, in the case of ^{19}F ($I = 1/2$) NMR investigations of the diluted antiferromagnet $\text{Mn}_{1-x}\text{Zn}_x\text{F}_2$, the $\ln[M_0 - M(t)]$ vs. $\ln(t)$ plot revealed that the experimental reality is the combination of Eq. (2) and Eq.(3) [24]. Furthermore, additional complications arise if $M(t)$ under consideration is not for $I = 1/2$. For example, ^{139}La is a spin $I = 7/2$ nucleus. In an ideal case of non-distributed $1/T_1$, $M(t)$ for the $I_z = -1/2 \leftrightarrow +1/2$ (i.e. central) transition of $I = 7/2$ can be written analytically as a linear combination of 4 normal modes [29, 30]:

$$M(t) = M_0 - A \sum_{k=1}^4 p_k e^{-q_k t/T_1}, \quad (4)$$

where $p_k = \{1/84, 3/44, 75/364, 1225/1716\}$ and $q_k = \{1, 6, 15, 28\}$, and $\sum_{k=1}^4 p_k = 1$ is normalized. In this case, the aforementioned log plot $\ln[M_0 - M(t)]$ does not yield a straight line, even if there is no distribution in $1/T_1$. Then how should we choose and justify the appropriate fitting function for $M(t)$ when $1/T_1$ is distributed and the fit with Eq. (4) is unsatisfactory? Should we just stretch each exponential term as in Eq. (2), or consider two or more values of $1/T_1$ as in Eq. (3)? Or a combination of both?

The ILTT₁ analysis technique tells us the answers to these questions. Regardless of the origin of the distribution of $1/T_1$ and its extent, one can actually *deduce* the probability density function $P(1/T_1)$ of $1/T_1$ based on the inverse Laplace transform (ILT) of $M(t)$ [31]. The ILT consists of fitting $M(t)$ to a sum of exponentials with decay rate $1/T_{1j}$ and weight $P(1/T_{1j}) \geq 0$. For the simplest case of $I = 1/2$, the discrete form of the ILT inverts for $P(1/T_1)$ assuming the following expression for the experimental data $M(t)$ [17–21]:

$$M(t) = \sum_{j=1}^m \left[1 - 2 e^{-t/T_{1j}} \right] P(1/T_{1j}). \quad (5)$$

For simplicity, we assumed perfect inversion (i.e. $A = 2M_0$). The summation $\sum_{j=1}^m P(1/T_{1j}) = M_0$ is the saturated value of the magnetization, and $m = 250$ is the chosen number of logarithmically-spaced bins in the $P(1/T_1)$ distribution. The normalization used to convert $P(1/T_1)$ into a probability density is detailed in subsection IV B. See the Supplemental Materials [32] as well as the references [17–21, 33–35] for the method to deal with the imperfect inversion in actual experimental data, the details of the mathematical background, and the general procedures for the ILT. Note that technically, Eq. (5) is the discrete form of a Fredholm integral equation of the first kind [36], but for simplicity we refer to it here as an ILT.

The advantage of ILT is that we need not assume a phenomenological functional forms for $M(t)$, such as Eq.

(2) or (3). The only assumption in the ILT is that $M(t)$ decays as a sum of exponentials with decay rates $1/T_{1j}$, implying a heterogeneous distribution in $1/T_1$ over the sample. If the distribution of $1/T_1$ is peaked at one value, $P(1/T_1)$ deduced from $M(t)$ will have one peak (i.e. be a delta function if $1/T_1$ has no distribution) at the most likely value of $1/T_1$. On the other hand, if $1/T_1$ is distributed around two distinctive values, as is the case for Eq. (3), $P(1/T_1)$ will have two peaks centered at $1/T_1^{fast}$ and $1/T_1^{slow}$.

It is useful to show how ILTT₁ analysis works based on a simple example. In Fig. 1(a), we generated a model relaxation curve $M(t)$ consisting of discrete data points represented by black dots. The best fit of the model data with Eq. (2) (red curve) yields $1/T_1^{str} = 1.44 \text{ s}^{-1}$ and $\beta = 0.89$. The fit seems very good, and the deviation from $\beta = 1$ is fairly small. Accordingly, one would be tempted to conclude that $P(1/T_1)$ is narrow and peaked around 1.5 s^{-1} , and hence may be close to a delta function as represented by the red vertical line in Fig. 1(b).

However in reality, we generated the discrete $M(t)$ data in Fig. 1(a) using a two component function as such:

$$M(t) = 1 - 2/3 e^{-3t} - 4/3 e^{-t}. \quad (6)$$

This is similar to the model in Eq. (3), with $1/T_1^{fast} = 3 \text{ s}^{-1}$, $1/T_1^{slow} = 1 \text{ s}^{-1}$, $M_o = 1$, $A_{fast} = 2/3$, and $A_{slow} = 4/3$, plus random noise at the level of 0.1% (i.e. a signal to noise ratio of $\text{SNR} = 1000$). The ILT of the model data in Fig. 1(a) results in $P(1/T_1)$ with double peaks at $1/T_1^{fast}$ and $1/T_1^{slow}$, as shown by a blue curve in Fig. 1(b). The log-mean (i.e. center of gravity on a log scale) of $P(1/T_1)$ is located at $1/T_1^{lm} = 1.48 \text{ s}^{-1}$ (represented by a dashed blue line). The finite width of the blue curve originates from the discreteness of the model data and the built-in random noise [32].

This simple example illustrates the power of ILT, and the potentially risky nature of the commonly used stretched exponential fit. While $1/T_1^{str}$ is indeed close to the real log-mean $1/T_1^{lm}$ of $P(1/T_1)$, the imagined distribution spectrum shown by a single vertical red line in Fig. 1(b) does not even remotely resemble the true, double peak structure in $P(1/T_1)$.

III. EXPERIMENTAL

We grew a single crystal sample of $\text{La}_{1.875}\text{Ba}_{0.125}\text{CuO}_4$ ($T_c = 4 \text{ K}$) based on the traveling solvent floating zone technique at Tohoku [6]. We aligned and cut a small piece of single crystal with the total mass of 51 mg for this study. We conducted ^{139}La NMR measurements at 9 T applied along the c -axis with the standard $\pi/2 - \pi$ spin-echo pulse sequence. The ^{139}La NMR lineshapes observed for the nuclear spin $I_z = +1/2 \leftrightarrow -1/2$ central transition were very similar to an earlier report [37].

We note that $\text{La}_{1.875}\text{Ba}_{0.125}\text{CuO}_4$ showed a partial loss of ^{139}La signal (i.e. partial ^{139}La wipeout) in the vicinity

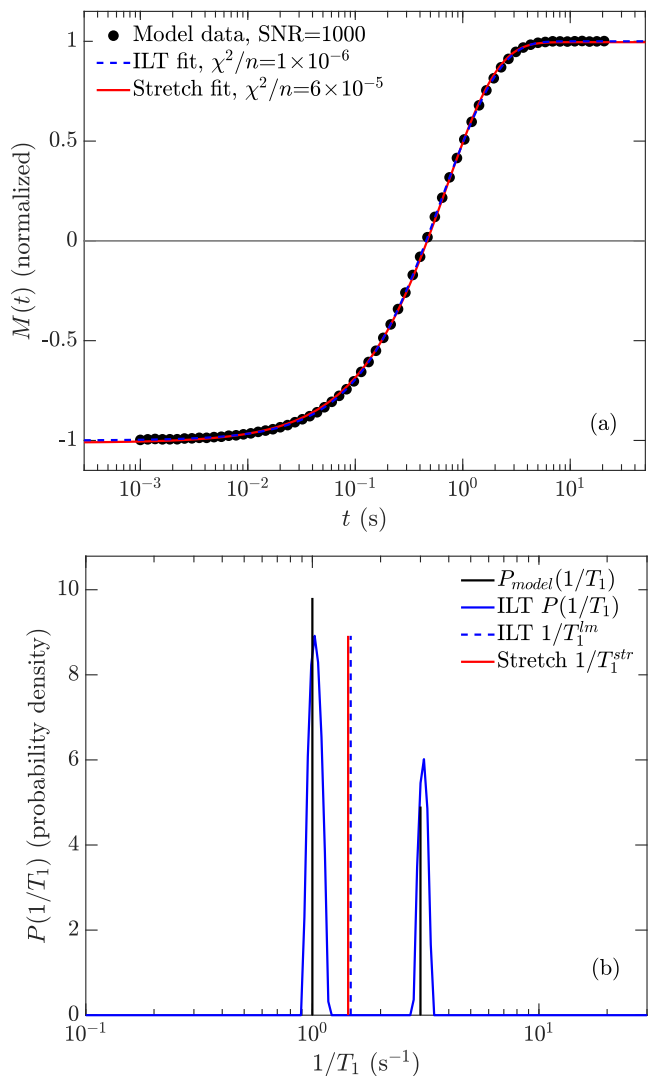


FIG. 1. (a) Model data $M(t)$ (\bullet), normalized by $M(t)/M_o$, generated for demonstration purposes using Eq. (6) as described in the main text, with $n = 64$ log-spaced data points. Solid red curve is the best stretched single exponential fit with Eq. (2) with $1/T_1^{str} = 1.44 \text{ s}^{-1}$ and $\beta = 0.89$, under the false assumption that there is only one peak in $P(1/T_1)$ centered around $1/T_1^{str}$. Dashed blue curve is the best ILT fit with Eq. (5) resulting in $P(1/T_1)$, represented by the blue curve in panel (b). Note how the ILT fit yields a lower mismatch χ^2/n than the stretched exponential fit. (b) Black vertical lines represent $P_{model}(1/T_1)$ from Eq. (6), consisting of two delta functions at $1/T_1^{fast}$ and $1/T_1^{slow}$. Blue curve represents the ILT spectrum $P(1/T_1)$ (probability density) of the $M(t)$ data points in (a). Notice that $1/T_1^{str}$ (red vertical line) is a good approximation of the log-mean $1/T_1^{lm}$ (dashed blue vertical line) of $P(1/T_1)$, however the stretched fit misses all of the detail in the underlying model $P(1/T_1)_{model}$.

of $\sim 35 \text{ K}$, where the signal dropped to $\sim 1/3$ of the full intensity. As such, the ILT may underestimate the distribution in fast $1/T_1$ components in the vicinity of ~ 35

K. This is similar to previous reports of ^{139}La wipeout in $\text{La}_{1.8-x}\text{Eu}_{0.2}\text{Sr}_x\text{CuO}_4$ (see Fig. 16 in [5]), but will not affect our conclusions. By contrast, $\text{La}_{1.885}\text{Sr}_{0.115}\text{CuO}_4$ showed no signs of ^{139}La wipeout for $T > T_c$ [22].

We measured $1/T_1$ using the inversion recovery method by applying a π pulse prior to the spin echo sequence. We summarize the representative results of $M(t)$ in Fig. 2. Measurements of $1/T_1^{str}$ with reasonable accuracy is an easy task, and can be usually completed in less than 1 hour at each temperature. However, the accuracy of $M(t)$ required for ILT is far less forgiving, because the resolution of the ILT curve $P(1/T_1)$ can depend on the experimental noise (i.e. the signal-to-noise ratio) of the $M(t)$ curve [32]. In addition, we had to use long spin echo recycling time up to 240 s between the spin-echo sequences, so that we can properly capture the longest components of $1/T_1$ in $M(t)$. For these reasons, it took up to 24 hours to measure $M(t)$ at a given temperature.

IV. ^{139}La NMR RESULTS AND DISCUSSIONS

A. Conventional stretched fit results $1/T_1^{str}$

Before we delve into the ILT analysis of the $M(t)$ data, let us first examine the consequence of the fit with the stretched exponential version of Eq. (4) commonly used in the literature:

$$M(t) = M_0 - A \sum_{k=1}^4 p_k e^{-(q_k t / T_1^{str})^\beta}, \quad (7)$$

where the same normal modes k [29, 30] are used as in Eq. 4, and $\sum_{k=1}^4 p_k = 1$ is normalized. We caution that, unlike the case of $I = 1/2$, there is no mathematical justification to place the same β in all four terms, although we will show below that this phenomenological procedure works fairly well to estimate the log-mean $1/T_1^{lm}$ of the underlying probability density function $P(1/T_1)$.

We summarize $1/T_1^{str}$ and β observed at the ^{139}La sites in Fig. 3(a) and (b), respectively. $1/T_1^{str}$ begins to increase sharply at T_{charge} , where charge order turns on a strong enhancement of low-frequency spin fluctuations in the charge ordered domains [4, 38]. Our finding is consistent with our powder NQR results by Hunt *et al.* [5] and a more recent single crystal NMR report by Baek *et al.* [37]. $1/T_1^{str}$ peaks around $T_{spin}^{\mu SR}$, and is progressively suppressed in the spin ordered state.

Note that $1/T_1^{str}$ is mildly enhanced near $T_{HTT-LTO} \simeq 236$ K, where β shows a minimum. This is not due to enhanced spin fluctuations, but rather to the contribution of slow EFG fluctuations near the structural phase transitions. A proof may be found in ^{63}Cu NMR measurements of $1/T_1$, which show no anomalies at $T_{HTT-LTO}$ [9, 11, 39]. $1/T_1$ is three orders of magnitude larger at the ^{63}Cu sites owing to much a stronger hyperfine coupling with Cu electron spins, and hence less sensitive to such slow EFG fluctuations

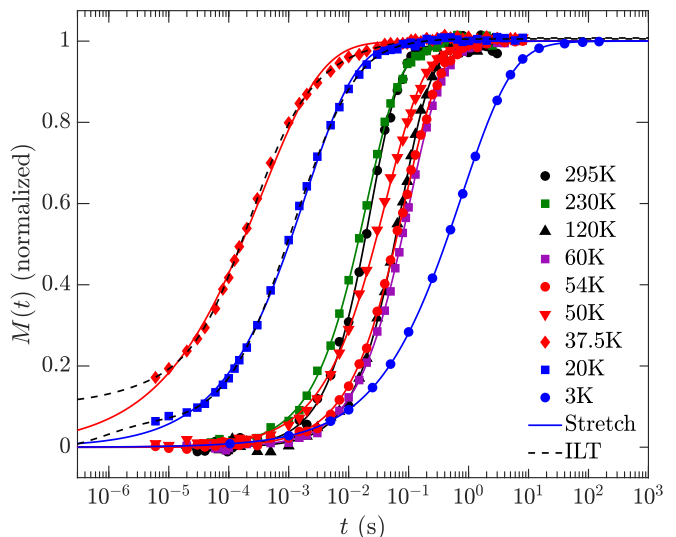


FIG. 2. ^{139}La NMR recovery curves $M(t)$ at representative temperatures, normalized by $(M(t) - M_0)/A + 1$, where M_0 and A are parameters from the best fits (solid curves) to the stretched exponential form in Eq. (7). Also shown are best fits to the ILT (dashed black lines) using Eq. (8) at 37.5 K and 20 K. Notice that the large distribution in $P(1/T_1)$ near $T_{spin}^{\mu SR}$ leads to poor stretched exponential fits at 37.5 K and 20 K, while the ILT yields good fits.

near the structural phase transition [9, 11, 39]. Strictly speaking, one cannot rely on Eq. (4) or (7) under the presence of EFG contributions to the T_1 process. This is because Eq. (4) or (7) implicitly assume that only the magnetic transitions with $\Delta I_z = \pm 1$ between two adjacent nuclear spin energy levels contribute to the T_1 process [29, 30], whereas the EFG fluctuations induce $\Delta I_z = \pm 2$ transitions as well. In practice, it is difficult to determine the spin and EFG induced $1/T_1$ contributions separately [40], and we phenomenologically rely on Eq. (7) to account for the enhanced $1/T_1$ due to the slowly fluctuating EFG.

Below $\simeq 200$ K down to $\simeq 80$ K, β is close to 1. This implies that the T_1 process is dominated by Cu spin fluctuations once the HTT-LTO structural phase transition is complete, and the distribution of $1/T_1$ is small. In the case of the superconducting compositions above $x \simeq 1/8$, $1/T_1$ continues to decrease smoothly toward T_c [37, 41, 42]. In contrast, $1/T_1^{str}$ in the present case begins to level off below $\simeq 80$ K, and β deviates from 1 again. In this temperature range, we expect a growth in nano-scale electronic inhomogeneity as we previously reported for $\text{La}_{2-x}\text{Sr}_x\text{CuO}_4$ [43]. In fact, we recently confirmed that $1/T_1$ at ^{63}Cu sites of the same $\text{La}_{1.875}\text{Ba}_{0.125}\text{CuO}_4$ crystal levels off below $\simeq 80$ K if measured with the pulse separation time $\tau = 2 \mu\text{s}$ between the 90 and 180 degree pulses, whereas $1/T_1$ keeps decreasing if measured with $\tau = 20 \mu\text{s}$ [39]. As such, our results below $\simeq 80$ K in Fig. 3 are consistent with

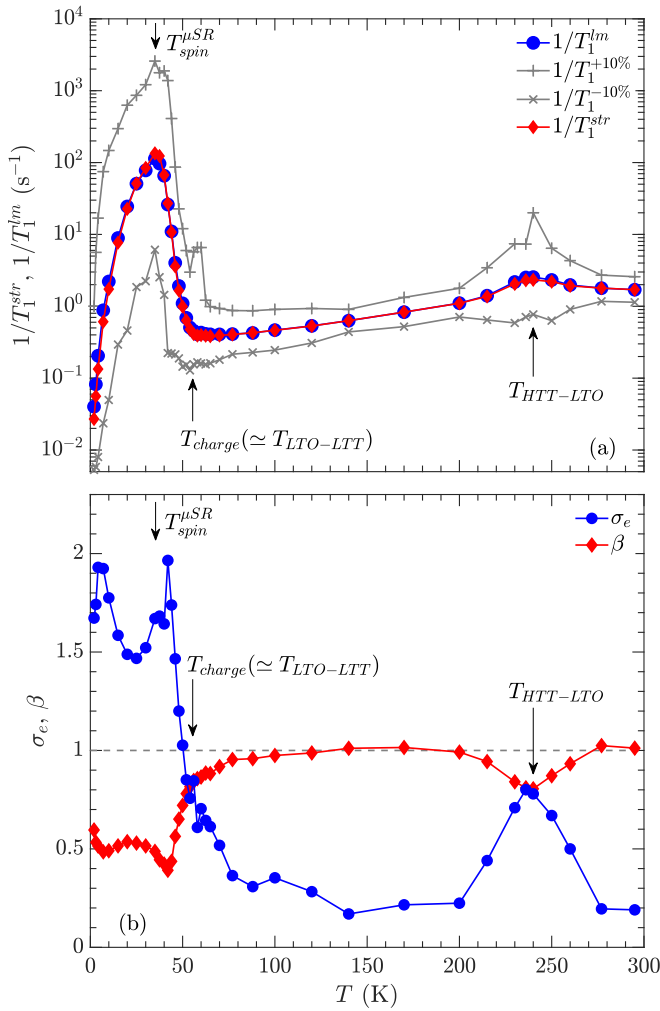


FIG. 3. (a) Temperature dependence of $1/T_1^{str}$ (red symbols) obtained from the stretched fit with Eq. (7), and log-mean value $1/T_1^{lm}$ (blue symbols) of the probability density $P(1/T_1)$ from Eq. (9), along with $1/T_1^{+10\%}$ ($1/T_1^{-10\%}$) at the top (bottom) 10% value of the distributed $P(1/T_1)$, respectively. $1/T_1^{str}$ may be considered a close approximation to $1/T_1^{lm}$. See Fig. 4 in [22] for the corresponding results observed for $\text{La}_{1.885}\text{Sr}_{0.115}\text{CuO}_4$. (b) Temperature dependence of the stretched exponent β , and standard deviation σ_e of $P(1/T_1)$ from Eq. 10. Note that σ_e and β are found to be anti-correlated [32].

enhanced spin fluctuations with growing spatial distributions. However, what about the potential influence of the dynamic short-range charge order observed above T_{charge} [8], and the slowing of phonons near the LTO to LTT transition toward T_{charge} ? The slowing fluctuations of charge and lattice would certainly induce slow EFG fluctuations that can potentially contribute to $1/T_1$, as observed near $T_{HTT-LTO}$. We will address this issue below based on ILT in subsection IV C.

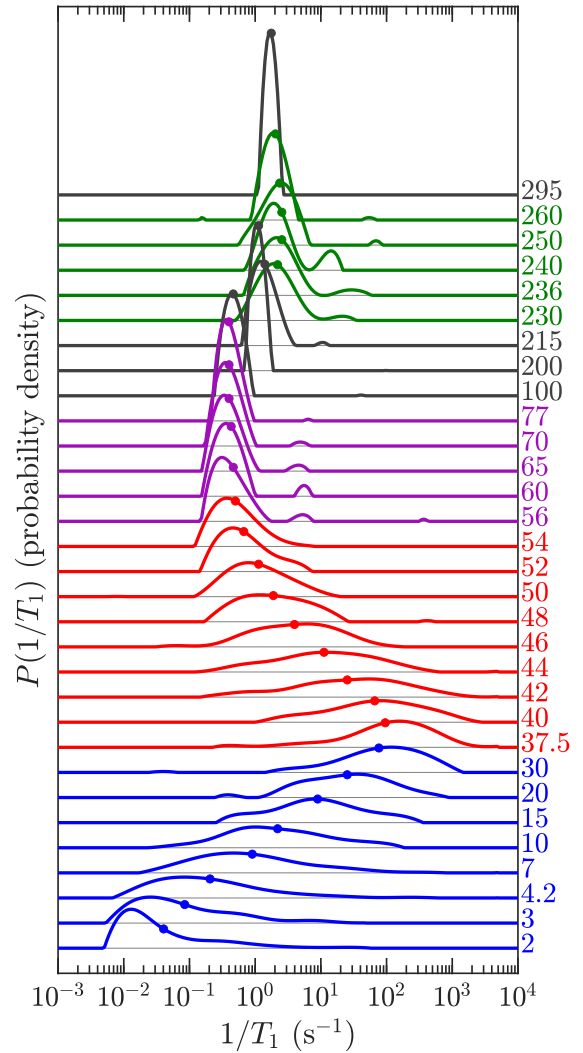


FIG. 4. Representative results of $P(1/T_1)$ (probability density) obtained from $M(t)$ based on ILT. For clarity, the origin of the vertical axes are shifted at each temperature, where the temperature T (K) is listed on the right-hand side. The location of the log-means $1/T_1^{lm}$ (\bullet) are shown on each $P(1/T_1)$.

B. The ILT results and consistency with the stretched fit

To account for the 4 normal modes for $I = 7/2$ in Eq. (4), we replaced Eq. (5) with the following:

$$M(t) = \sum_{j=1}^m \sum_{k=1}^4 \left[1 - 2p_k e^{-q_k t / T_{1j}} \right] P(1/T_{1j}), \quad (8)$$

where the same normal modes k [29, 30] are used as in Eq. (4), and $\sum_{k=1}^4 p_k = 1$ is normalized. The summation $\sum_{j=1}^m P(1/T_{1j}) = M_0$ is the saturated value of the magnetization, and $m = 250$ is the chosen number of logarithmically-spaced bins ranging from $10^{-3} \text{ s}^{-1} \leq 1/T_{1j} \leq 10^5 \text{ s}^{-1}$. The probability density is then nor-

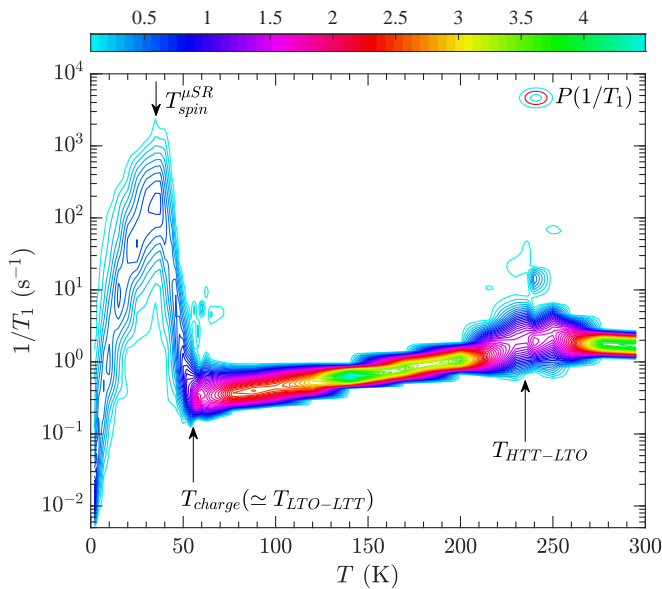


FIG. 5. Contour map of $P(1/T_1)$ (probability density) generated from ILT, using 64 contours. Color bar scale is shown at the top of the figure.

malized to $\sum_{j=1}^m P(1/T_{1j}) \Delta_P = 1$, where the constant $\Delta_P = \log_{10}(1/T_{1j+1}) - \log_{10}(1/T_{1j}) = 0.0321$ is the logarithmic bin spacing. This normalization ensures a 1-1 comparison of $P(1/T_1)$'s when the bin spacing is different for each $P(1/T_1)$. Using a \log_{10} base to define Δ_P conveniently yields unit area for a square $P(1/T_1)$ distribution a decade wide and of unit height.

In Fig. 4, we summarize the ILT curves $P(1/T_1)$ obtained from $M(t)$ at representative temperatures. We also show the evolution of $P(1/T_1)$ with temperature in the color contour map in Fig. 5. From each of these ILT curves, we deduced $1/T_1^{lm}$ and σ_e , the log-mean of the distribution $P(1/T_1)$ and the log-standard deviation of $1/T_1$, respectively, as such:

$$\ln(1/T_1^{lm}) = \sum_{j=1}^m \ln(1/T_{1j}) P(1/T_{1j}) \Delta_P, \quad (9)$$

$$\sigma_e^2 = \sum_{j=1}^m [\ln(1/T_{1j}) - \ln(1/T_1^{lm})]^2 P(1/T_{1j}) \Delta_P, \quad (10)$$

where $\sum_{j=1}^m P(1/T_{1j}) \Delta_P = 1$. We use the subscript e in σ_e to emphasize that the logarithm to base e (i.e. the natural logarithm) is used to compute the log-standard deviation. We summarize $1/T_1^{lm}$ in comparison to $1/T_1^{str}$ in Fig. 3(a), while σ_e is compared with β in Fig. 3(b). $1/T_1^{str}$ and $1/T_1^{lm}$ agree well. That is, $1/T_1^{str}$ estimated from the phenomenological stretch fit may be considered as a good approximation for the average value of the distributed $1/T_1$. σ_e also shows clear anti-correlation with β . This also makes sense. β becomes smaller than 1 when $1/T_1$ develops a distribution, whereas σ_e increases when

the distribution of $1/T_1$ grows and $P(1/T_1)$ becomes wider. Thus we have established that our ILT results encompass the equivalent information as the stretched exponential analysis of $M(t)$. Note however that besides $1/T_1^{str}$ and β , the stretched exponential analysis loses all other information about the underlying probability density $P(1/T_1)$. In the Supplemental Materials [32] we present details of the ILT analysis, including the concept of “resolution” and uncertainties in $P(1/T_1)$.

C. Distribution of $1/T_1$

Having established the validity of the ILT, let us take an additional step and look into exactly how the distribution of $1/T_1$ develops. At the top of Fig. 4 is $P(1/T_1)$ result at 295 K shown in dark gray. $P(1/T_1)$ is single-peaked, with the log-mean at $1/T_1^{lm} = 1.7 \text{ s}^{-1}$. Note that the stretched exponential fit of $M(t)$ returns $\beta = 1.01$ at 295 K, and hence the distribution of $1/T_1$ is minimal. The finite width of $P(1/T_1)$ at 295 K primarily originates from the finite signal-to-noise ratio of the measurement [32].

We summarize the $P(1/T_1)$ curves in the vicinity of $T_{HTT-LTO} \simeq 235 \text{ K}$ in green in Fig. 4. Two noticeable changes take place near $T_{HTT-LTO}$. First, the main peak of $P(1/T_1)$ shifts to the right, accompanied by significant broadening. The small shift corresponds to the small increase observed for $1/T_1^{lm}$ as well as $1/T_1^{str}$. The broadening is a consequence of the additional transitions caused by EFG fluctuations, which are not explicitly taken into account in Eq. (8). Second, a small but noticeable split-off peak consistently emerges with $1/T_1 \simeq 20 \text{ s}^{-1}$. Note that this does not necessarily mean that the EFG induced transition has an order of magnitude faster $1/T_1$ in a small volume fraction of the sample. As noted above, the additional contributions by the fluctuating EFG to the relaxation processes with $\Delta I_z = \pm 1$ and ± 2 could significantly modify the relaxation function itself; we take this effect into account only phenomenologically in Eq.(8) which is derived for purely magnetic relaxation. The slow EFG fluctuations cease to exist when the second order structural phase transition is complete, and the split-off peak disappears as we go deeper into the LTO structure below $T_{HTT-LTO}$. $P(1/T_1)$ regains a narrower, single-peaked structure at 215 K and below down to 100 K, as shown by dark gray curves.

The ILT results from $\simeq 80 \text{ K}$ down to $T_{charge} \simeq 54 \text{ K}$ are shown in purple. We recall that the charge order transition is accompanied by a nearly first order LTO to LTT structural phase transition [6, 8]. Interestingly, a split-off peak analogous to that observed around $T_{HTT-LTO}$ emerges again, signaling the presence of slow EFG fluctuations at the NMR frequency scale. In a separate study based on ^{63}Cu NMR, we show that ^{63}Cu NMR lineshape exhibits strong magnetic broadening in this temperature range below $\simeq 80 \text{ K}$ prior to the onset of long range charge order at T_{charge} . Moreover, ^{63}Cu $1/T_1$ begins to

distribute [39]. Taken together, these findings suggest that, regardless of the exact origin of the slow EFG fluctuations above T_{charge} detected here, spin correlations grow hand in hand with the slow lattice and/or charge fluctuations below $\simeq 80$ K.

We use red curves to show the ILT results in the charge ordered state below $T_{charge} \simeq 54$ K down to the spin ordering temperature $T_{spin}^{\mu SR} \simeq 35$ K. At 54 K, the split-off peak due to EFG fluctuations is suppressed. This is consistent with the nearly first-order nature of the simultaneous LTT and charge order transitions [6, 8]. Once entering the long range charge ordered state, $P(1/T_1)$ begins to broaden asymmetrically by transferring some spectral weight to larger values of $1/T_1$. At 48 K, approximately 1/3 of the spectral weight still remains at $1/T_1 \simeq 1$ s⁻¹ or below, although the fastest component reaches $1/T_1 \simeq 30$ s⁻¹. In other words, not all the Cu spin fluctuations begin to slow down and enhance $1/T_1$ immediately below T_{charge} . Upon further cooling, the entire $P(1/T_1)$ curve shifts to larger values of $1/T_1$ while increasing in width. All ¹³⁹La nuclear spins relax with highly enhanced $1/T_1$ by 37 K, followed by spin ordering at $T_{spin}^{\mu SR} \simeq 35$ K. A physical picture that emerges from these observations is that *the volume fraction of the canonically behaving segments of CuO₂ planes with slow $1/T_1$ values gradually decreases below T_{charge} , and the spin order at the relatively slow measurement time scale of μ SR experiments sets in when $\sim 100\%$ volume fraction of the CuO₂ planes is under the influence of enhanced spin fluctuations triggered by charge order.*

We summarize the ILT results below $T_{spin}^{\mu SR}$ using blue curves. The ILT curve $P(1/T_1)$ progressively shifts its weight to lower values of $1/T_1$ as the fluctuating spins freeze toward the base temperature. By 7 K, a majority of ¹³⁹La sites relax with $1/T_1 \simeq 1$ s⁻¹ or slower. It is in this temperature range where Zeeman perturbed ⁶³Cu NQR signals become observable with increasing intensity [5, 10], since the hyperfine magnetic field from frozen Cu moments become static at the NMR measurement time scale. In a separate work, we will demonstrate that a cut off introduced for $P(1/T_1)$ can naturally account for the fraction of the observable ⁶³Cu NMR signal intensity that arises from canonically behaving domains below T_{charge} , *i.e.* ⁶³Cu signal intensity wipe out effects [39].

D. Comparison with La_{1.885}Sr_{0.115}CuO₄

In Fig. 6, we compare the $P(1/T_1)$ results for La_{1.875}Ba_{0.125}CuO₄ with our earlier report for La_{1.885}Sr_{0.115}CuO₄ [22]. $P(1/T_1)$ for La_{1.885}Sr_{0.115}CuO₄ begins to broaden below the onset of its charge order at $T_{charge} \simeq 80$ K [44–46], without exhibiting the split-off peak arising from EFG fluctuations. Since no LTT structural phase transition exists in La_{1.885}Sr_{0.115}CuO₄, this might be an indication that the signature of the EFG fluctuations observed above T_{charge} in the present case of La_{1.875}Ba_{0.125}CuO₄ is due primarily to the slow lat-

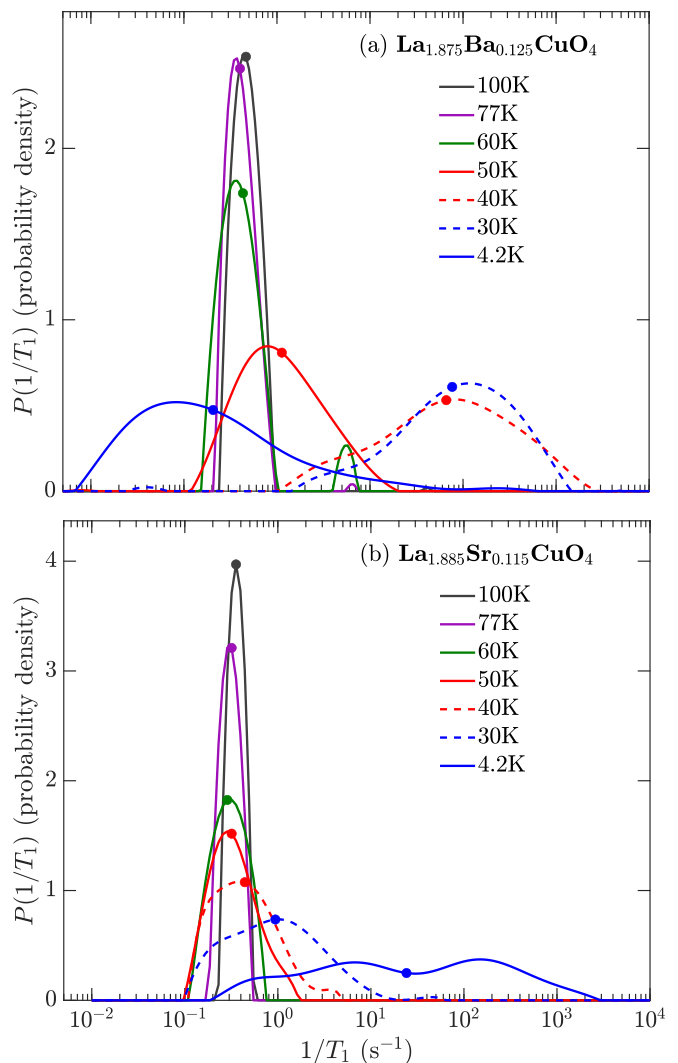


FIG. 6. Comparison of the $P(1/T_1)$ (probability density) between (a) La_{1.875}Ba_{0.125}CuO₄ (this work, $T_{charge} \simeq 54$ K, $T_c = 4$ K) and, (b) La_{1.885}Sr_{0.115}CuO₄ (adopted from [47], $T_{charge} \simeq 80$ K, $T_c = 31$ K), at selected temperatures. The location of the log-means $1/T_1^{lm}$ (●) are shown on each $P(1/T_1)$.

tice fluctuations rather than slow charge fluctuations. On the other hand, the Bragg peaks associated with charge order in La_{1.885}Sr_{0.115}CuO₄ are known to be very weak, and hence charge fluctuations may also be too weak to induce the split-off peak in $P(1/T_1)$.

Another interesting aspect is the qualitative difference in the way the distribution of $P(1/T_1)$ develops. In the case of La_{1.885}Sr_{0.115}CuO₄, notice that $P(1/T_1)$ continues to transfer its spectral weight to smaller values down to $1/T_1 \simeq 0.1$ s⁻¹ even below $T_{charge} \simeq 80$ K, although the log-mean of the distribution is shifting to larger values of $1/T_1$. This means that $1/T_1$ continues to become smaller at a substantial fraction of ¹³⁹La sites even deep inside the charge ordered state below $T_{charge} \simeq 80$ K. The temperature dependence of $1/T_1$ at these ¹³⁹La sites is

qualitatively the same as that in the canonical superconducting CuO_2 planes in $\text{La}_{1.85}\text{Sr}_{0.15}\text{CuO}_4$ [37, 41, 42]. It is just that the *volume fraction* of such canonically superconducting domains gradually decreases below T_{charge} . As a consequence, we can clearly see that the peak structure from the canonically behaving domains is still visible as a clearly identifiable shoulder at $1/T_1 \simeq 0.1 \text{ s}^{-1}$ down to $\sim 30 \text{ K}$. This conclusion was corroborated by the fact that two types of ^{63}Cu NMR signals exist in $\text{La}_{1.885}\text{Sr}_{0.115}\text{CuO}_4$, too: the wing like signal is extremely broad and with large $1/T_1$, whereas the canonically behaving signal has a narrow lineshape with slow $1/T_1$ that is comparable to the optimally doped superconductor with $x = 0.15$ [48].

In contrast, the slow shoulder at $1/T_1 \simeq 0.1 \text{ s}^{-1}$ observed for $\text{La}_{1.885}\text{Sr}_{0.115}\text{CuO}_4$ is not observable in the present case of $\text{La}_{1.875}\text{Ba}_{0.125}\text{CuO}_4$. As temperature decreases below $T_{charge} \simeq 54 \text{ K}$, $P(1/T_1)$ shifts to larger values of $1/T_1$ more quickly. There is only a hint of a slow shoulder at $1/T_1 \simeq 3 \text{ s}^{-1}$ from 54 K down to 48 K in Fig. 4. We confirmed that the ^{63}Cu NMR lineshape for $\text{La}_{1.875}\text{Ba}_{0.125}\text{CuO}_4$ broadens more homogeneously below $\simeq 80 \text{ K}$, and lacks the aforementioned two component wing plus narrow-peak structure observed for $\text{La}_{1.885}\text{Sr}_{0.115}\text{CuO}_4$ [39]. In short, CuO_2 planes in $\text{La}_{1.875}\text{Ba}_{0.125}\text{CuO}_4$ are more homogeneously affected by charge order and accompanying enhancements of slow spin fluctuations, which increases $1/T_1$.

V. SUMMARY AND CONCLUSIONS

We have reported the ILTT₁ analysis to demonstrate how the distribution of $1/T_1$ develops in charge ordered $\text{La}_{1.875}\text{Ba}_{0.125}\text{CuO}_4$. We identified the signature of the slow EFG fluctuations near $T_{HTT-LTO}$, and showed that the same signature reemerges above T_{charge} . Our experiments and ILTT₁ analysis cannot determine whether the source of the slow EFG fluctuations is the lattice and/or charge vibrations.

By comparing the probability density function $P(1/T_1)$ from ILTT₁ analysis, we demonstrated that the magnetic properties of the CuO_2 planes become highly inhomogeneous below $T_{charge} \simeq 54 \text{ K}$, and domains with canonical behavior of a high T_c superconductor persist even below T_{charge} . These residual domains are oblivious to the charge order transition, and spin fluctuations are not anomalously enhanced. This suggests that charge order does not set in homogeneously at T_{charge} in the entire CuO_2 planes. This finding is consistent with the fact that the width of the charge order Bragg peaks (*i.e.* the inverse of the charge order correlation length) is not resolution limited above $\simeq 40 \text{ K}$, and hence the size of the charge ordered domains is not infinite [8].

The volume fraction of these residual domains gradually diminishes below $T_{charge} \simeq 54 \text{ K}$ in $\text{La}_{1.875}\text{Ba}_{0.125}\text{CuO}_4$. By 40 K , nearly $\simeq 100\%$ volume of the CuO_2 planes have large $1/T_1$ induced by enhanced

low frequency Cu spin fluctuations triggered by charge order. This finding is in stark contrast with the case of $\text{La}_{1.885}\text{Sr}_{0.115}\text{CuO}_4$, where a significant fraction of domains in the CuO_2 planes still exhibits characteristic behavior of high T_c superconductor with slowing $1/T_1$ at 40 K [22, 47]. These contrasting behaviors are consistent with the fact that superconductivity sets in at as high as $T_c = 31 \text{ K}$ for $\text{La}_{1.885}\text{Sr}_{0.115}\text{CuO}_4$, while superconductivity is strongly suppressed to $T_c = 4 \text{ K}$ in $\text{La}_{1.875}\text{Ba}_{0.125}\text{CuO}_4$.

The present work also highlights the usefulness of the ILTT₁ analysis technique in general. The ILT provides us with much richer information than the conventional stretched fit analysis since ILT generates the probability density function $P(1/T_1)$ rather than just the average value of $1/T_1$. Moreover, it is important to note that ILTT₁ analysis is unbiased, and one does not need to assume the shape of the distribution function $P(1/T_1)$. The novel ILTT₁ analysis, which has been used successfully in NMR petrophysics, has the potential to revolutionize NMR research of quantum materials with disorder.

Finally, we briefly comment on some earlier publications, in which several groups tried to model the distribution of $1/T_1$ in cuprates [5, 49, 50] and unrelated materials [51, 52]. Note that all these earlier attempts were made by assuming a functional form of $P(1/T_1)$ up front, which may or may not reflect the reality. For example, our earlier attempt in 2001 assumed a symmetrical Gaussian distribution of $1/T_1$ on a log scale in the charge ordered state of cuprates for fitting $M(t)$, as shown in Fig. 12 of [5]. The present work shows that such a symmetrical functional form is only approximately true for $\text{La}_{1.875}\text{Ba}_{0.125}\text{CuO}_4$ in a limited temperature range, and invalid for $\text{La}_{1.885}\text{Sr}_{0.115}\text{CuO}_4$ [22]. Ref. [49] assumed instead that magnetic inhomogeneity of the CuO_2 planes in Eu co-doped 214 cuprates is caused entirely by pre-existing quenched disorder, which gives rise to a Gaussian distribution in an activation energy for spin fluctuations rather than the distribution of $1/T_1$ itself. Since their toy model is based on an incorrect assumption that charge order transition does not exist, all the NMR properties are expected to evolve smoothly, in contradiction with the experimental reality such as Fig. 3(a). Ref. [50] extended our earlier analysis in [5], and assumed a symmetrical distribution function for $1/T_1$ on a log scale for $\text{La}_{1.88}\text{Sr}_{0.12}\text{CuO}_4$ [50]. Despite the unrealistic assumption in contradiction to the experimental reality of non-symmetric $P(1/T_1)$ [22], their analysis actually showed the onset of unusual NMR anomalies starting from $\simeq 80 \text{ K}$. However, the authors in Ref. [50] did not attribute their findings to the onset of charge order, as they had been advocating for the absence of charge order in the superconducting phase of $\text{La}_{2-x}\text{Sr}_x\text{CuO}_4$.

ACKNOWLEDGMENTS

The authors thank J. Wang for helpful discussions. P.M.S. is supported by The Rice University Consortium for Processes in Porous Media. The work at McMaster is supported by NSERC. The work at Tohoku is supported by Grant-in-Aid for Scientific Research (A) (16H02125), Japan.

Supplemental Materials

VI. INVERSE LAPLACE TRANSFORM

The inverse Laplace transform (ILT) consists of fitting the measured inversion recovery curve $M(t)$ to a sum of exponentials with decay rate $1/T_{1j}$ and weight $P(1/T_{1j}) \geq 0$. The advantage of ILT over stretched exponential fits is that the ILT does not assume any phenomenological functional forms for the decay in $M(t)$. The only assumption in the ILT is that $M(t)$ decays as a sum of exponentials with decay rates $1/T_{1j}$, implying a heterogeneous distribution in $1/T_1$ over the sample. Put in other words, $P(1/T_1)$ is the probability density function for $1/T_1$ over the heterogeneous sample.

In the case of ^{139}La nuclear spin with $I = 7/2$, we need to take into account four normal modes in the $1/T_1$ relaxation process [29, 30]. The discrete form of the ILT inverts for $P(1/T_{1j})$ assuming the following expression for the experimental data $M(t)$ measured at a set of time t_i :

$$M(t_i) = \sum_{j=1}^m \sum_{k=1}^4 \left[1 - 2p_k e^{-q_k t_i / T_{1j}} \right] P(1/T_{1j}) + E(t_i). \quad (11)$$

The coefficients $\{p_k, q_k\}$ (with $k = 1, \dots, 4$) are calculated for each of the aforementioned normal modes [29, 30] as such $p_k = \{1/84, 3/44, 75/364, 1225/1716\}$ and $q_k = \{1, 6, 15, 28\}$, and $\sum_{k=1}^4 p_k = 1$ is normalized. $E(t)$ is Gaussian noise with standard deviation σ_E . Technically, Eq. 11 is the discrete form of a Fredholm integral equation of the first kind [36], but for simplicity we refer to it as an ILT.

The summation $\sum_{j=1}^m P(1/T_{1j}) = M_0$ in Eq. 11 is the saturated value of the magnetization, and m is the chosen number of logarithmically-spaced bins in the $P(1/T_1)$ distribution. The probability density is then normalized to $\sum_{j=1}^m P(1/T_{1j}) \Delta_P = 1$, where the constant $\Delta_P = \log_{10}(1/T_{1j+1}) - \log_{10}(1/T_{1j})$ is the logarithmic bin spacing. This normalization ensures a 1-1 comparison of $P(1/T_1)$'s when the bin spacing is different for each $P(1/T_1)$. Using a \log_{10} base to define Δ_P conveniently yields unit area for a square $P(1/T_1)$ distribution a decade wide and of unit height.

The column vector form for Eq. 11 is given by:

$$\mathbf{M} = K \mathbf{P} + \mathbf{E}, \quad \mathbf{P} \geq 0, \quad (12)$$

where the following are defined:

$$\begin{aligned} \mathbf{M} &= \{M(t_i), i = 1, \dots, n\}, \\ K &= \left\{ K_{ij} = \sum_{k=1}^4 \left[1 - 2p_k e^{-q_k t_i / T_{1j}} \right] \right\}, \\ \mathbf{P} &= \{P(1/T_{1j}), j = 1, \dots, m\}, \end{aligned} \quad (13)$$

where K is the kernel matrix of size $n \times m$, and \mathbf{E} is the noise vector. The number of measured data points in the

present case is between $n = 18 \leftrightarrow 46$, and m is chosen to be $m = 250$. For computational efficiency, the kernel K is compressed using singular value decomposition (SVD) [17–19], which is not detailed here in the interest of brevity. However, given the relatively small size of the K matrix ($n \times m \simeq 46 \times 250$ typically), there is no need for data compression in the present case.

The disadvantage of ILT is that it is an ill-posed problem in the sense that for a given set of data with finite noise E , many solutions will fit the data within the statistics of the noise. Various solutions exist to deal with such ill-posed problems [19], including Tikhonov regularization [17, 18, 20, 21, 53], maximum entropy [33], Monte Carlo [34], and the Mellin transform [35].

In this report we choose the Tikhonov regularization method given the extensive literature on the subject. Regarding uncertainties in the optimal solution \mathbf{P} , we note that there are no uncertainties or “error bars” associated with each bin j of the $P(1/T_{1j})$ distribution. Instead, uncertainties in the moments of \mathbf{P} such as $1/T_1^{lm}$ (log-mean) or σ_e (log standard deviation) can be quantified. Furthermore, uncertainties in the total area of \mathbf{P} (i.e. $\sum_{j=1}^m P(1/T_{1j}) = M_0$) and the partial area of \mathbf{P} below (i.e. $\sum_{j=1}^{m,cut} P(1/T_{1j})$) or above (i.e. $\sum_{j=m,cut}^m P(1/T_{1j})$) a certain a cutoff $(1/T_1)_{cut}$ can also be quantified. Details of how to quantify these uncertainties can be found in [34, 35], which are beyond the scope in this report.

A. Non-negative optimization

Using the Tikhonov regularization method, the goal is to find the solution \mathbf{P} which minimizes the cost function [53]:

$$\mathbf{P} = \arg \min_{\mathbf{P} \geq 0} \|\mathbf{M} - K \mathbf{P}\|^2 + \alpha \|\mathbf{P}\|^2 \quad (14)$$

by using non-negative least-squares, where $\|\cdot\|$ is the vector norm. The first term is the residual between data and fit, and the second term is the regularization factor. α is the scalar regularization parameter (i.e. a smoothing factor) chosen to be large enough to make the solution stable in the presence of noise. The solution $\mathbf{P}(\alpha)$ in Eq. 14 implicitly depends on α . Choosing $\alpha = 0$ leads to a unique solution $\mathbf{P}(\alpha = 0)$, however the solution is “spiky”, where the position and amplitude of the spikes depend on the particular noise realization \mathbf{E} ; this undesirable case is so called “under-regularized”. In the opposite extreme, choosing a large $\alpha \gg 10$ over-smooths the solution $\mathbf{P}(\alpha \gg 10)$; this undesirable case is so called “over-regularized”.

The first task in finding the optimal solution \mathbf{P} in Eq. 14 is to choose a reasonable range of $1/T_{1j}$ bins for $P(1/T_{1j})$. Given the large distribution in $P(1/T_{1j})$ at low temperatures, and given the range of times $10^{-5} \text{ s} \lesssim t_i \lesssim 10^2 \text{ s}$ in $M(t_i)$, we selected $m = 250$ bins equally spaced on a logarithmic scale ranging from $10^{-3} \text{ s}^{-1} \leq 1/T_{1j} \leq 10^5 \text{ s}^{-1}$. This results in a logarithmic bin spacing of

$\Delta_P = \log_{10}(1/T_{1j+1}) - \log_{10}(1/T_{1j}) = 0.0321$. Note that using a log-spaced distribution function $P(1/T_{1j})$ implies that the equivalent linear-spaced distribution function is given by $P_{lin}(1/T_{1j}) = P(1/T_{1j})/(1/T_{1j})$.

Details of the steps required to optimize the non-negative solution \mathbf{P} in Eq. 14 can be found in [17, 53]. The basic steps for the 1D case without SVD decomposition are shown here for convenience. The function $f(\mathbf{c})$ to be minimized with respect to the vector \mathbf{c} is defined as:

$$f(\mathbf{c}) = \frac{1}{2} \mathbf{c}' [G(\mathbf{c}) + \alpha I] \mathbf{c} - \mathbf{c}' \mathbf{M}, \quad (15)$$

where the quasi-Newton method [54] can be used, with an initial guess of $\mathbf{c} = \mathbf{1}$, and \mathbf{c}' represents the transpose of \mathbf{c} . The \mathbf{c} vector is the same size as \mathbf{M} . I is the identity matrix of size $\mathbf{M} \times \mathbf{M}$. The “ G matrix” of size $\mathbf{M} \times \mathbf{M}$ is defined as:

$$G(\mathbf{c}) = K \begin{bmatrix} H(K'_1 \mathbf{c}) & 0 & \dots & 0 \\ 0 & H(K'_2 \mathbf{c}) & \dots & 0 \\ \vdots & \vdots & \dots & \vdots \\ 0 & 0 & \dots & H(K'_m \mathbf{c}) \end{bmatrix} K' \quad (16)$$

where H is the heavy-side function, and K_j is the j th column of K .

With the optimal \mathbf{c} now found, the optimal non-negative solution \mathbf{P} is given by:

$$\mathbf{P} = \max \{0, K' \mathbf{c}\}, \quad (17)$$

which is a function of α . The next step is to determine the optimal regularization parameter α_{opt} to be used.

B. Optimal regularization parameter

The residual $\chi(\alpha)$ between data and optimal fit is given by:

$$\chi(\alpha) = \alpha \|\mathbf{c}\| = \|\mathbf{M} - K \mathbf{P}(\alpha)\|. \quad (18)$$

There are then two criteria for establishing α_{opt} :

$$\begin{aligned} \chi(\alpha_1) &= \sigma_E \sqrt{n}, \\ \left. \frac{d \ln \chi(\alpha)}{d \ln \alpha} \right|_{\alpha_2} &= 10^{-1}, \\ \alpha_{opt} &= \max \{ \alpha_1, \alpha_2 \}. \end{aligned} \quad (19)$$

The first criterion is the Bulter-Reeds-Dawson (BRD) condition [53], where α_1 is found such that $\chi(\alpha_1)$ equals the noise σ_E times the square-root of the number of data points \sqrt{n} (or the square-root of the number of singular values $\sqrt{n_{SVD}}$ if SVD is used). The experimental noise σ_E can be determined using one of the following techniques: (1) acquiring $M(t)$ data with the RF power turned off, then taking the standard deviation of the data, (2) using the standard deviation of the imaginary channel in $M(t)$,

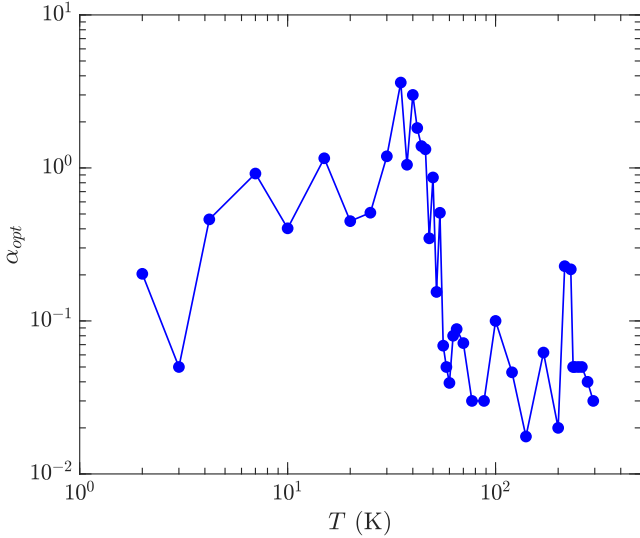


FIG. 7. Temperature dependence of the optimal regularization parameter α_{opt} .

although there may be ringing artifacts, or (3) using SVD and taking the standard deviation of the difference between the data and the projection of the data onto the range space [17].

The BRD condition works well provided $M(t)$ is dominated by statistical noise $E(t)$. However, if systematic errors occur in $M(t)$, then the BRD condition breaks down. Systematic errors occur due to hardware limitations which are only apparent at high SNR, or the kernel K may not be exact due to the presence of quadrupole relaxation. In such cases, a second criterion is introduced known as the “heel” condition [18], where α_2 is defined when the derivative $d\ln\chi(\alpha)/d\ln\alpha$ is equal to 10^{-1} . A derivative of 10^{-1} corresponds roughly to the heel of the $\chi(\alpha)$ versus α function, where $d\ln\chi(\alpha)/d\ln\alpha > 0$ for $\alpha \geq \alpha_{opt}$.

The optimal alpha α_{opt} is then obtained from the maximum of both conditions $\max\{\alpha_1, \alpha_2\}$. In practice, Eq. 14 is solved for a range of selected values $\alpha = 10^6 \rightarrow 10^{-3}$ in descending half-decade (or finer) steps, with the misfit $\chi(\alpha)$ and slope $d\ln\chi(\alpha)/d\ln\alpha$ calculated at each descending step. In order to save computational time, the α descent can be stopped once either α_1 or α_2 has been reached. Another way to save computation time during the α descent is to use the optimal \mathbf{c} vector from the previous α computation as the initial guess of the next α computation in Eq. 15.

Fig. 7 shows the temperature dependence of α_{opt} for the dataset, which indicate that α_{opt} increases somewhat at temperatures below $\lesssim 50$ K. This is a result of the heel condition ($\alpha_{opt} = \alpha_2$) being met more often than the BRD condition ($\alpha_{opt} = \alpha_1$).

C. Incomplete inversion at short times

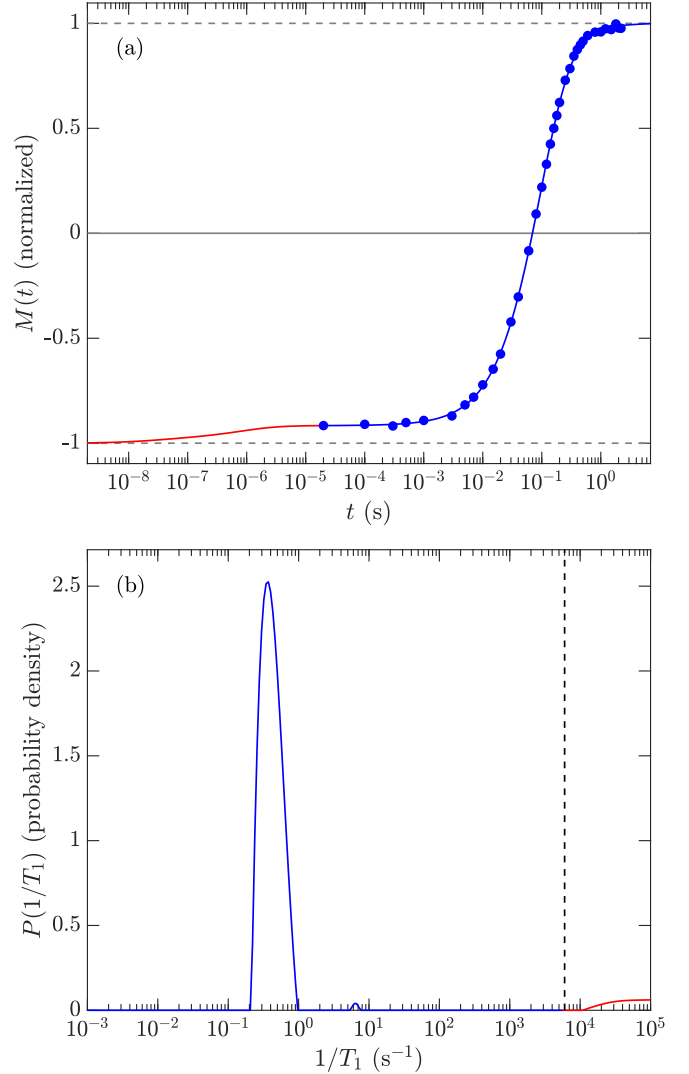


FIG. 8. (a) Magnetization data $M(t)$ (\bullet) and ILT fit (solid curve) at 77 K, where red region ($t < t_{min}$) shows incomplete inversion. (b) Corresponding ILT distribution $P(1/T_1)$ (solid curve) at 77 K, where red region indicates unphysical region $1/T_1 > (1/T_1)_{cut}$ (dashed line) used to account for incomplete inversion in $M(t)$.

Due to experimental limitations, the inversion recovery following the 180° r.f. pulse is not exact. One way to take this into account is to replace the factor of 2 in Eq. 11 with a free parameter whose optimized value ends up less than 2.

A more robust method for accounting for incomplete inversion is to use the $P(1/T_1)$ distribution itself. The selection of bins $10^{-3} \text{ s}^{-1} \leq 1/T_{1j} \leq 10^5 \text{ s}^{-1}$ in $P(1/T_{1j})$ is chosen to have an extended range at the fast end $(1/T_1)_{max} = 10^5 \text{ s}^{-1}$. These fast bins simulate fast relaxation components that decay well be-

fore the first data point at $t_{min} \simeq 10^{-5}$ s, specifically $\sum_k p_k e^{-q_k t_{min} (1/T_1)_{max}} \simeq 0.005$. While these fast $1/T_1$ components are not physically measurable, they mimic the effect of incomplete inversion of the magnetization at $M(t_{min} \simeq 10^{-5}$ s).

An example of the incomplete inversion in $M(t)$ is shown in Fig. 8(a) for 77 K, where the red part of the curve ($t < t_{min}$) shows the incomplete inversion. The corresponding $P(1/T_1)$ is shown in Fig. 8(b), where the red part of the curve shows the region $1/T_1 > (1/T_1)_{cut}$, where $(1/T_1)_{cut} = 6000 \text{ s}^{-1}$ is chosen. The region $P(1/T_1 > (1/T_1)_{cut})$ is a fraction $\simeq 0.04$ of the total $P(1/T_1)$ at 77 K, which accounts for the incomplete inversion of $M(t_{min})/M_0 \simeq -0.92$. $(1/T_1)_{cut}$ is chosen for each measurement, i.e. at each temperature, based on the extent of the fast region.

Figure 9 shows the temperature dependence of the fraction of signal $P(1/T_1 > (1/T_1)_{cut})$. We do not see a systematic variation in $P(1/T_1 > (1/T_1)_{cut})$ with temperature, in particular it does not correlate with the partial ^{139}La wipeout temperature in the vicinity of ~ 35 K. Rather, $P(1/T_1 > (1/T_1)_{cut})$ is a function of various acquisition parameters and experimental conditions.

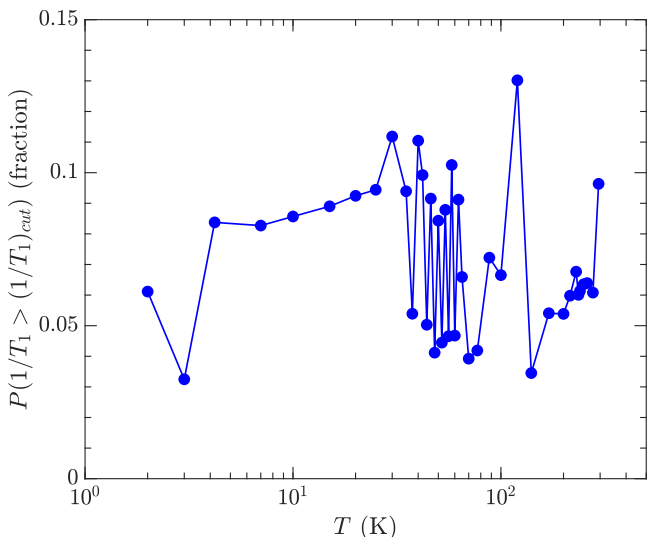


FIG. 9. Temperature dependence of the fraction of signal above the cutoff $P(1/T_1 > (1/T_1)_{cut})$ due to incomplete inversion recovery.

The final step is to truncate the data in the unphysical region $P(1/T_{1j} > (1/T_1)_{cut})$ by setting those bins to zero, i.e. $P(1/T_{1j} > (1/T_1)_{cut}) = 0$. In other words, the effect of incomplete inversion is not used in the subsequent analysis of $P(1/T_1)$.

D. Resolution as a function of SNR

It is helpful to get a sense of the “resolution” in $P(1/T_1)$, as a function of the signal to noise ratio

(SNR) in $M(t)$. For this purpose, a forward model $P_{model}(1/T_{1j})$ is generated comprising two log-normal peaks at $1/T_{1j} = 1 \text{ s}^{-1}$ and $1/T_{1j} = 10^2 \text{ s}^{-1}$ with equal amplitudes and equal widths. The $M(t)$ data are then generated using Eq. 11 with synthetic Gaussian noise σ_E . The above inversion is then carried out using three different noise values σ_E , or equivalently, three different SNR’s defined as:

$$\text{SNR} = \frac{M_0}{\sigma_E}. \quad (20)$$

The resulting distributions as a function of SNR are shown in Fig. 10, where the selected values $\text{SNR} = \{50, 150, 1000\}$ correspond roughly to the lowest, average, and highest SNR values of the experimental data (see Fig. 11) respectively

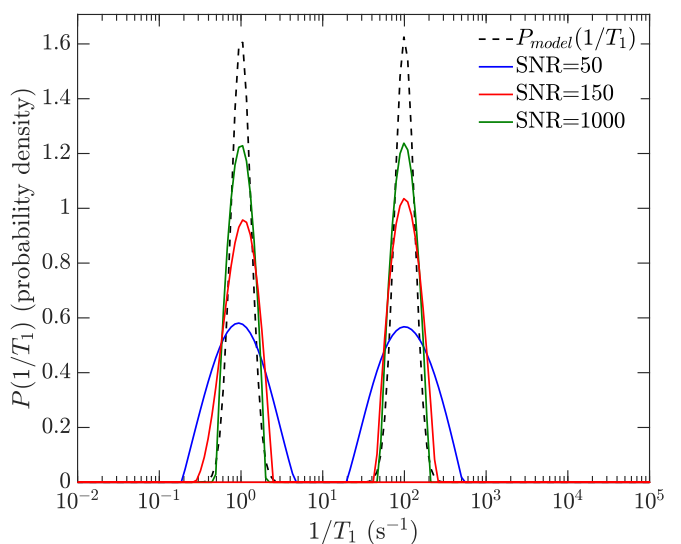


FIG. 10. Forward model $P_{model}(1/T_1)$, and inverted distributions as a function of SNR. The optimal values for α_{opt} are $\alpha_{opt} = \{0.9, 0.03, 0.006\}$ for $\text{SNR} = \{50, 150, 1000\}$, respectively.

Fig. 10 indicates that the resolution in the inverted distributions increases with increasing SNR, as expected. In other words, the inverted distributions tend more towards $P_{model}(1/T_1)$ at higher SNR, which is a result of the lower α_{opt} found from the BRD criterion in Eq. 19 (i.e. lower σ_E). The forward model example illustrates the capability of the ILT in separating peaks in $P(1/T_1)$ as a function of SNR. In the case of the lowest $\text{SNR} = 50$, the peaks are distinguishable provided they are a half-decade apart in $1/T_1$. As such, a half-decade in $1/T_1$ may loosely be considered as the ILT “resolution” at $\text{SNR} = 50$, although this is only semi-quantitative.

As shown in Fig. 10, the resolution can in principle improve with increasing SNR. Fig. 11 shows the temperature dependence of the SNR for the experimental data, which indicates that a resolution of less than a half-decade in $1/T_1$ is possible below $\lesssim 50$ K, provided

the BRD condition ($\alpha_{opt} = \alpha_1$) is met rather than the heel condition ($\alpha_{opt} = \alpha_2$). If the heel condition is met, then increasing the SNR does not necessarily improve the resolution.

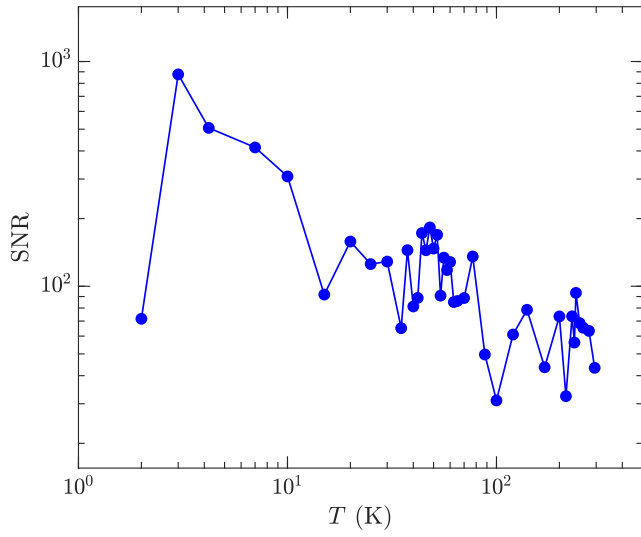


FIG. 11. Temperature dependence of the SNR for the experimental data.

VII. COMPARISON BETWEEN ILT AND STRETCHED EXPONENTIAL

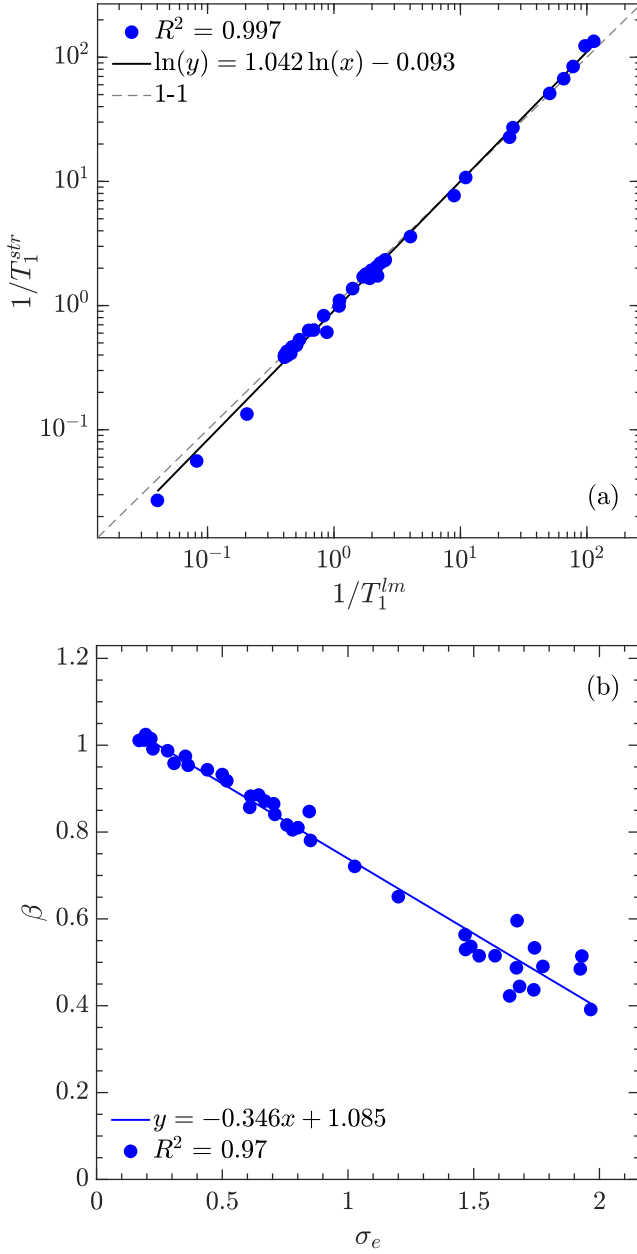


FIG. 12. (a) Cross plot of log-mean $1/T_1^{lm}$ from ILT versus $1/T_1^{str}$ from stretched fit. (b) Cross plot of standard deviation σ_e from ILT versus stretched exponent β from stretched fit.

Fig. 12 shows a cross plot the ILT results versus the stretched exponential results. As shown in Fig. 12(a), a very strong correlation ($R^2 = 0.997$) is found between the log-mean $1/T_1^{lm}$ and the stretched $1/T_1^{str}$. While in Fig. 12(b), a strong anti-correlation ($R^2 = 0.970$) is found between the log-mean standard-deviation σ_e and the stretched exponent β . Note however that besides $1/T_1^{str}$ and β , the stretched exponential analysis loses all other information about the underlying probability density $P(1/T_1)$. Furthermore, when $P(1/T_1)$ is wide, i.e. when β is small ($\beta \lesssim 0.6$), the stretched exponential fit does not necessarily give a good fit to $M(t)$, which results in scattering of σ_e versus β in Fig. 12(b).

-
- [1] J. D. Axe, A. H. Moudden, D. Hohlwein, D. E. Cox, K. M. Mohanty, A. R. Moodenbaugh, and Y. Xu, Structural phase transformations and superconductivity in $\text{La}_{2-x}\text{Ba}_x\text{CuO}_4$, Phys. Rev. Lett. **62**, 2751 (1989).
 [2] G. M. Luke, L. P. Le, B. J. Strenlieb, W. D. Wu, Y. J. Ue-

- mura, J. H. Brewer, and Riseman, Static magnetic order in $\text{La}_{1.875}\text{Ba}_{0.125}\text{CuO}_4$, Physica C **185-189**, 1175 (1991).
 [3] J. M. Tranquada, B. J. Sternlieb, J. D. Axe, Y. Nakamura, and S. Uchida, Evidence for stripe correlations in copper oxide superconductors, Nature **375**, 561 (1995).

- [4] A. W. Hunt, P. M. Singer, K. R. Thurber, and T. Imai, ^{63}Cu NQR measurement of stripe order parameter in $\text{La}_{2-x}\text{Sr}_x\text{CuO}_4$, *Phys. Rev. Lett.* **82**, 4300 (1999).
- [5] A. W. Hunt, P. M. Singer, A. F. Cederström, and T. Imai, Glassy slowing of stripe modulation in $(\text{La}, \text{Eu}, \text{Nd})_{2-x}(\text{Sr}, \text{Ba})_x\text{CuO}_4$: a ^{63}Cu and ^{139}La NQR study down to 350 mK, *Phys. Rev. B* **64**, 134525 (2001).
- [6] M. Fujita, H. Goka, K. Yamada, J. M. Tranquada, and L. P. Regnault, Stripe order, depinning, and fluctuations in $\text{La}_{1.875}\text{Ba}_{0.125}\text{CuO}_4$ and $\text{La}_{1.875}\text{Ba}_{0.075}\text{Sr}_{0.050}\text{CuO}_4$, *Phys. Rev. B* **70**, 104517 (2004).
- [7] V. Thampy, X. M. Chen, Y. Cao, C. Mazzoli, A. M. Barbour, W. Hu, H. Miao, G. Fabbri, R. D. Zhong, G. D. Gu, J. M. Tranquada, I. K. Robinson, S. B. Wilkins, and M. P. M. Dean, Static charge-density-wave order in the superconducting state of $\text{La}_{2-x}\text{Ba}_x\text{CuO}_4$, *Phys. Rev. B* **95**, 241111 (2017).
- [8] H. Miao, R. Fumagalli, M. Rossi, J. Lorenzana, G. Seibold, F. Yakhov-Harris, K. Kummer, N. B. Brookes, G. D. Gu, L. Braicovich, G. Ghiringhelli, and M. P. M. Dean, Formation of incommensurate charge density waves in cuprates, *Phys. Rev. X* **9**, 031042 (2019).
- [9] T. Imai, K. Yoshimura, T. Uemura, H. Yasuoka, and K. Kosuge, ^{63}Cu NMR study of spin dynamics in $\text{La}_{2-x}(\text{Sr}, \text{Ba})_x\text{CuO}_y$ ($0.04 \leq x \leq 0.16$, $3.99 \leq y \leq 4.03$), *J. Phys. Soc. Jpn.* **59**, 3846 (1990).
- [10] H. Tou, M. Matsumura, and H. Yamagata, Anomalous Cu-NQR spectral change due to low-temperature structural transition around $x = 0.06$ in $(\text{La}_{1-x}\text{Ba}_x)_2\text{CuO}_4$, *J. Phys. Soc. Jpn.* **61**, 1477 (1992).
- [11] H. Tou, M. Matsumura, and H. Yamagata, ^{63}Cu nuclear spin-lattice relaxation study for low-temperature structural transition in $(\text{La}_{1-x}\text{Ba}_x)_2\text{CuO}_4$ around $x = 0.06$, *J. Phys. Soc. Jpn.* **62**, 1474 (1993).
- [12] K. Kumagai, K. Kawano, I. Watanabe, K. Nishiyama, and K. Nagamine, μSR and NMR investigations on electronic and magnetic state around $x = 0.12$ in $\text{La}_{2-x}\text{Sr}_x\text{CuO}_4$ and $\text{La}_{2-x}\text{Ba}_x\text{CuO}_4$, *Hyperfine Interactions* **86**, 473 (1994).
- [13] T. Goto, S. Kazama, K. Miyagawa, and T. Fukase, $^{63}/^{65}\text{Cu}/^{139}\text{La}$ -NMR study on antiferromagnetic ordering in high- T_c oxides $\text{La}_{2-x}\text{Sr}_x\text{CuO}_4$ ($x \simeq 0.115$) and $\text{La}_{2-x}\text{Ba}_x\text{CuO}_4$ ($x \simeq 0.125$), *J. Phys. Soc. Jpn.* **63**, 3494 (1994).
- [14] S.-H. Baek, Y. Utz, M. Hücker, G. D. Gu, B. Büchner, and H.-J. Grafe, Magnetic field induced anisotropy of ^{139}La spin-lattice relaxation rates in stripe ordered $\text{La}_{1.875}\text{Ba}_{0.125}\text{CuO}_4$, *Phys. Rev. B* **92**, 155144 (2015).
- [15] D. Pelc, H.-J. Grafe, G. D. Gu, and M. Požek, Cu nuclear magnetic resonance study of charge and spin stripe order in $\text{La}_{1.875}\text{Ba}_{0.125}\text{CuO}_4$, *Phys. Rev. B* **95**, 054508 (2017).
- [16] D. C. Johnston, S.-H. Baek, X. Zong, F. Borsa, J. Schmalian, and S. Kondo, Dynamics of magnetic defects in heavy fermion LiV_2O_4 from stretched exponential ^7Li NMR relaxation, *Phys. Rev. Lett.* **95**, 176408 (2005).
- [17] L. Venkataraman, Y.-Q. Song, and M. D. Hürlimann, Solving fredholm integrals of the first kind with tensor product structure in 2 and 2.5 dimensions, *IEEE Trans. Sig. Process.* **50** (5), 1017 (2002).
- [18] Y.-Q. Song, L. Venkataraman, M. D. Hürlimann, M. Flaum, P. Frulla, and C. Straley, T_1 - T_2 correlation spectra obtained using fast two-dimensional laplace inversion, *J. Magn. Reson.* **154**, 261 (2002).
- [19] J. Mitchell, T. C. Chandrasekera, and L. Gladden, Numerical estimation of relaxation and diffusion distributions in two dimensions, *Prog. Nucl. Magn. Reson. Spect.* **62**, 34 (2012).
- [20] P. M. Singer, D. Asthagiri, Z. Chen, A. Valiya Parambathu, G. J. Hirasaki, and W. G. Chapman, Role of internal motions and molecular geometry on the NMR relaxation of hydrocarbons, *J. Chem. Phys.* **148** (16), 164507 (2018).
- [21] P. M. Singer, D. Asthagiri, W. G. Chapman, and G. J. Hirasaki, NMR spin-rotation relaxation and diffusion of methane, *J. Chem. Phys.* **148** (20), 204504 (2018).
- [22] A. Arsenault, T. Imai, P. M. Singer, K. M. Suzuki, and M. Fujita, Magnetic inhomogeneity in charge ordered $\text{La}_{1.885}\text{Sr}_{0.115}\text{CuO}_4$ investigated by NMR, accepted for publication in *Phys. Rev. B* (arXiv:1912.11448).
- [23] S. K. Takahashi, J. Wang, A. Arsenault, T. Imai, M. Abramchuk, F. Tafti, and P. M. Singer, Spin excitations of a proximate kitaev quantum spin liquid realized in Cu_2IrO_3 , *Phys. Rev. X* **9**, 031047 (2019).
- [24] M. Itoh, H. Yasuoka, A. R. King, and V. Jaccarino, Decay of the Nuclear Magnetization in the Randomly Diluted Antiferromagnets $\text{Fe}_x\text{Zn}_{1-x}\text{F}_2$ and $\text{Mn}_x\text{Zn}_{1-x}\text{F}_2$, *J. Phys. Soc. Jpn.* **55**, 964 (1986).
- [25] P. Thayamballi and D. Hone, Nuclear Relaxation in a Randomly Diluted Heisenberg Paramagnet, *Phys. Rev. B* **21**, 1766 (1980).
- [26] T. Imai, T. Shimizu, H. Yasuoka, Y. Ueda, and K. Kosuge, Nuclear spin-lattice relaxation of $^{63,65}\text{Cu}$ at the Cu(2) sites of the high T_c superconductor $\text{YBa}_2\text{Cu}_3\text{O}_{7-\delta}$, *J. Phys. Soc. Jpn.* **57**, 2280 (1988).
- [27] T. Imai, T. Shimizu, H. Yasuoka, Y. Ueda, and K. Kosuge, Anomalous Temperature dependence of Cu Nuclear Spin-Lattice Relaxation in $\text{YBa}_2\text{Cu}_3\text{O}_{6.91}$, *J. Phys. Soc. Jpn.* **57**, 2280 (1988).
- [28] T. Imai, H. Yasuoka, T. Shimizu, Y. Ueda, K. Yoshimura, and K. Kosuge, Cu spin dynamics in high T_c and related oxides investigated by nuclear spin-lattice relaxation, *Physica C* **162-164**, 169 (1989).
- [29] E. R. Andrew and D. P. Tunstall, Spin-Lattice Relaxation in Imperfect Cubic Crystals and in Non-cubic Crystals, *Proceedings of the Royal Society* **78**, 1 (1961).
- [30] A. Narath, Nuclear spin-lattice relaxation in hexagonal transition metals: Titanium, *Phys. Rev.* **162**, 320 (1967).
- [31] P. M. Singer, D. Asthagiri, W. G. Chapman, and G. J. Hirasaki, NMR spin-rotation relaxation and diffusion of methane, *The Journal of Chemical Physics* **148**, 204504 (2018), <https://doi.org/10.1063/1.5027097>.
- [32] See supplementary material available at [url] for technical details of ILT.
- [33] E. Chouzenoux, S. Moussaoui, J. Idier, and F. Mariette, Efficient maximum entropy reconstruction of nuclear magnetic resonance T_1 - T_2 spectra, *IEEE Trans. Sig. Process.* **58** (12), 6040 (2010).
- [34] M. Prange and Y.-Q. Song, Quantifying uncertainty in NMR T_2 spectra using Monte Carlo inversion, *J. Magn. Reson.* **196**, 54 (2009).
- [35] L. Venkataraman, F. K. Gruber, T. M. Habashy, and D. E. Freed, Mellin transform of CPMG data, *J. Magn. Reson.* **206**, 20 (2010).
- [36] E. J. Fordham, L. Venkataraman, J. Mitchell, and

- A. Valori, What are, and what are not inverse Laplace transforms, *Diffusion Fundam.* **29**, 1 (2017).
- [37] S.-H. Baek, A. Erb, and B. Büchner, Low-energy spin dynamics and critical hole concentrations in $\text{La}_{2-x}\text{Sr}_x\text{CuO}_4$ ($0.07 \leq x \leq 0.2$) revealed by ^{139}La and ^{63}Cu nuclear magnetic resonance, *Phys. Rev. B* **96**, 094519 (2017).
- [38] J. M. Tranquada, N. Ichikawa, and S. Uchida, Glassy nature of stripe ordering in $\text{La}_{1.6-x}\text{Nd}_{0.4}\text{Sr}_x\text{CuO}_4$, *Phys. Rev. B* **59**, 14712 (1999).
- [39] T. Imai, A. Arsenault, P. M. Singer, and M. Fujita, Revisiting ^{63}Cu NMR evidence for charge order in $\text{La}_{1.875}\text{Ba}_{0.125}\text{CuO}_4$, Submitted to *Phys. Rev. B* (2019).
- [40] A. Suter, M. Mali, J. Roos, and D. Brinkmann, Mixed magnetic and quadrupolar relaxation in the presence of a dominant static zeeman hamiltonian, *Journal of Physics: Condensed Matter* **10**, 5977 (1998).
- [41] T. Kobayashi, S. Wada, Y. Kitaoka, and K. Asayama, Nuclear spin-lattice relaxation of ^{139}La in superconducting $(\text{La}_{1-x}\text{Sr}_x)_2\text{CuO}_4$, *J. Phys. Soc. Jpn.* **58**, 2662 (1989).
- [42] K. Yoshimura, T. Uemura, M. Kato, T. Shibata, K. Kosuge, T. Imai, and H. Yasuoka, Magnetic phase differentiation in the $\text{La}_{2-x}\text{Sr}_x\text{CuO}_y$ systems -Cu and La nuclear quadrupole resonance and relaxation, *Springer Proceedings in Physics* **60**, 405 (1992).
- [43] P. M. Singer, A. W. Hunt, and T. Imai, ^{63}Cu NQR evidence for spatial variation of hole concentration in $\text{La}_{2-x}\text{Sr}_x\text{CuO}_4$, *Phys. Rev. Lett.* **88**, 047602 (2002).
- [44] T. P. Croft, C. Lester, M. S. Senn, A. Bombardi, and S. M. Hayden, Charge density wave fluctuations in $\text{La}_{2-x}\text{Sr}_x\text{CuO}_4$ and their competition with superconductivity, *Phys. Rev. B* **89**, 224513 (2014).
- [45] V. Thampy, M. P. M. Dean, N. B. Christensen, L. Steinke, Z. Islam, M. Oda, M. Ido, N. Momono, S. B. Wilkins, and J. P. Hill, Rotated stripe order and its competition with superconductivity in $\text{La}_{1.88}\text{Sr}_{0.12}\text{CuO}_4$, *Phys. Rev. B* **90**, 100510 (2014).
- [46] J. Wen, H. Huang, S. J. Lee, H. Jang, J. Knight, Y. S. Lee, M. Fujita, K. M. Suzuki, S. Asano, S. A. Kivelson, C. C. Kao, and J.-S. Lee, Observation of two types of charge-density wave orders in superconducting $\text{La}_{2-x}\text{Sr}_x\text{CuO}_4$, *Nature Communications* **10**, 3269 (2019).
- [47] A. Arsenault, S. K. Takahashi, T. Imai, W. He, Y. S. Lee, and M. Fujita, ^{139}La NMR investigation of the charge and spin order in a $\text{La}_{1.885}\text{Sr}_{0.115}\text{CuO}_4$ single crystal, *Phys. Rev. B* **97**, 064511 (2018).
- [48] T. Imai, S. K. Takahashi, A. Arsenault, A. W. Acton, D. Lee, W. He, Y. S. Lee, and M. Fujita, Revisiting ^{63}Cu NMR evidence for charge order in superconducting $\text{La}_{1.885}\text{Sr}_{0.115}\text{CuO}_4$, *Phys. Rev. B* **96**, 224508 (2017).
- [49] N. J. Curro, P. C. Hammel, B. J. Suh, M. Hücker, B. Büchner, U. Ammerahl, and A. Revcolevschi, Inhomogeneous low frequency spin dynamics in $\text{La}_{1.65}\text{Eu}_{0.2}\text{Sr}_{0.15}\text{CuO}_4$, *Phys. Rev. Lett.* **85**, 642 (2000).
- [50] V. F. Mitrović, M.-H. Julien, C. de Vaulx, M. Horvatić, C. Berthier, T. Suzuki, and K. Yamada, Similar glassy features in the ^{139}La NMR response of pure and disordered $\text{La}_{1.88}\text{Sr}_{0.12}\text{CuO}_4$, *Phys. Rev. B* **78**, 014504 (2008).
- [51] J. Gezo, T.-K. Lui, B. Wolin, C. P. Slichter, R. Giannetta, and J. A. Schlueter, Stretched exponential spin relaxation in organic superconductors, *Phys. Rev. B* **88**, 140504 (2013).
- [52] A. P. Dioguardi, M. M. Lawson, B. T. Bush, J. Crocker, K. R. Shirer, D. M. Nisson, T. Kissikov, S. Ran, S. L. Bud'ko, P. C. Canfield, S. Yuan, P. L. Kuhns, A. P. Reyes, H.-J. Grafe, and N. J. Curro, NMR evidence for inhomogeneous glassy behavior driven by nematic fluctuations in iron arsenide superconductors, *Phys. Rev. B* **92**, 165116 (2015).
- [53] J. P. Butler, J. A. Reeds, and S. V. Dawson, Estimating solutions of first kind integral equations with non-negative constraints and optimal smoothing, *SIAM J. Numer. Anal.* **18**(3), 381 (1981).
- [54] C. Lawson and R. Hanson, *Solving Least Squares Problems* (Prentice-Hall, Englewood Cliffs, NJ, 1974).